Reconfigurable Acoustic Absorber Comprising Flexible Tubular Resonators for Broadband Sound Absorption

Ryohei Tsuruta, Xiaopeng Li, Ziqi Yu, Hideo Iizuka, and Taehwa Lee*
Toyota Research Institute of North America, Toyota Motor North America, Ann Arbor, Michigan 48105, USA

(Received 21 March 2022; revised 9 May 2022; accepted 27 May 2022; published 22 July 2022)

Typical acoustic metamaterial absorbers rely on relatively rigid materials for acoustic resonances, which, however, poses a challenge in reshaping and reconfiguring them. Here, we demonstrate soft reconfigurable acoustic absorbers, which are realized by the use of flexible tubular resonators. Owing to the structural compliance, the tube absorbers promote intriguing acoustic-structure coupling and exhibit hybrid resonances of acoustic and structural modes, which are characterized by Rabi splitting in the strong-coupling regime and Fano-like resonance in the weak-coupling regime. Also, the soft walls of the flexible resonators induce decreased resonance frequencies for low-frequency absorption by reducing the effective sound speed inside the tube. Moreover, we find that these hybrid resonances are critically influenced by the structural loss of the flexible resonators. While elucidating the role of the material rigidity and structural loss in acoustic resonances, this work allows us to design versatile broadband absorbers that can be reconfigured depending on the topology of a target substrate.

DOI: 10.1103/PhysRevApplied.18.014055

I. INTRODUCTION

Broadband sound absorption is extremely useful in various practical and scientific applications requiring a reduction of acoustic reflection and transmission for accurate sensing and noise suppression [1–3]. Sound barriers made of porous or rigid materials are widely implemented to meet the requirement. However, these barriers, which obey the mass law, inevitably become bulky and heavy to control low-frequency sound, thus motivating acoustic metamaterial research for compact subwavelength acoustic absorbers. Considerable progress has been made in acoustic metamaterial absorbers, which have extreme characteristics such as ultrathin structures [4–7], ultrabroadband absorption [8–12], and extremely low-frequency absorption (<100 Hz) [13,14]. These extreme attributes are realized by synergistic use of multiple-resonance and space-coiling approaches. Alternatively, broadband absorption is attained by employing a few heavily damped resonances for maximizing the bandwidth of each resonance [15,16]. Besides such extreme features, acoustic metamaterials have evolved to tunable multifunctional absorbers, e.g., ventilated absorbers [17–19] permitting air flow as well as blocking sound propagation [20–24].

The aforementioned acoustic metamaterials exclusively use high-rigidity materials (e.g., plastics and metals) to define air cavities and channels by rigid walls for Helmholtz and quarter-wavelength resonators. Because the structural modes of the high-rigidity walls are typically decoupled to acoustic modes, analysis of these metamaterials is simply carried out by solving the wave equation for acoustic waves in the air domains without considering the structural response. Also, such high-rigidity walls of acoustic resonators are advantageous over compliant walls, suppressing unwanted wave leakages across the soft walls. In addition, these rigid metamaterial absorbers of complicated structures take advantage of additive prototyping such as three-dimensional (3D) printing [25]. Despite these merits, flexible materials for acoustic metamaterial absorbers can be a great choice to further enhance the acoustic performance by inducing additional resonance modes and to use the material rigidity as a tuning knob for control of acoustic-structure interaction. Furthermore, the flexible metamaterials can be reconfigured in response to external stimulus (e.g., stretching and deformation), offering a tunable control of their characteristics. Particularly, membrane-type resonators are made of thin flexible membranes for low-frequency sound absorption [2]. Yet, while requiring a rigid backing, they rely on structural resonances alone, exhibiting a relatively narrow bandwidth due to high-quality factor resonances and low losses.

Employing soft materials for other types of resonators such as Helmholtz resonators (HRs) or quarter-wavelength resonators (QWRs) is promising by inducing additional structural resonances on top of acoustic modes. Also, constructing metamaterials with flexible HRs and QWRs benefits from physical understanding of existing rigid metamaterial absorbers based on QWRs or HRs. The

*taehwa.lee@toyota.com

fundamental question arises whether the use of flexible materials compromises acoustic performance by increasing acoustic transmission. To answer the question, the effects of the structural rigidity and loss need to be systematically investigated. Only a limited number of studies are available focusing on HRs with either part or whole of the compliant walls [26–28].

In this work, we demonstrate reconfigurable metamaterial absorbers composed of flexible tube resonators supporting acoustic QWR modes. The flexible tube resonators having a very low rigidity exhibit an additional absorption peak induced by acoustic-structure coupling (structural mode), which is located close to the peak corresponding to the QWR mode, demonstrating weak or strong coupling depending on the proximity between the two modes. The multiple absorption peaks are well captured by an analytical model based on the axisymmetric shell motion equation. Moreover, the structural damping of the flexible tube critically influences the structural and QWR modes by increasing the effective acoustic energy loss. With these soft-tube resonators, we show two types of broadband absorbers to take advantage of their low rigidity for reconfiguration. First, a wall-type absorber is constructed, consisting of multiple tube resonators of different lengths. In addition, the flexible resonators are employed for duct silencers. Our reconfigurable absorbers can be useful in various applications while providing physical insight into acoustic-structure coupling phenomena.

II. RESULTS AND DISCUSSION

A. Analytical model for acoustic-structure coupling in flexible tubular quarter-wavelength resonator

The reconfigurable sound absorber consists of a flexible circular tube attached to a rigid square plate, as shown in Fig. 1(a). The inner diameter ($2r_i$) of the tube is the same as the diameter of the hole in the plate. The flexible tube, closed at the distal end by a rigid cap, constitutes a QWR, whose resonance frequency f_{QWR} is determined by the tube length (L), i.e., $f_{\mathrm{QWR}} \approx 0.25nc/L$ with c being the sound speed and n being the odd number. Besides the acoustic resonance, the flexible tubes permit considerable wall vibration, exhibiting structural resonance modes close to the acoustic QWR mode. Unlike rigid walls, the flexible tubes may induce wave transmission across their flexible walls while the square plate, made of a metal, is sufficiently rigid such that no acoustic transmission occurs through the plate. The acoustic absorber based on flexible tubes enables us to readily tune the acoustic resonance by using cut-to-size tubes. In addition, by having multiple tubes of different lengths, the absorption bandwidth can be increased, as the broadband absorber with 16 tubular resonators is shown in Fig. 1(b). Moreover, the flexibility of the tubes allows them to be reconfigured depending on a target substrate of an arbitrary geometry.

To model flexible tubes (radius r_i and thickness h) aligned to the z direction, we consider axisymmetric vibrations, meaning that the longitudinal and radial motions are not coupled to the torsional motion. The equation of motion for the longitudinal (u) and radial (w) displacements is represented as [29,30]

$$\frac{\partial^2 u}{\partial z^2} + \frac{\nu}{a}\frac{\partial w}{\partial z} + \frac{\omega^2}{a^2\omega_a^2}u = 0, \tag{1a}$$

$$\frac{\nu}{a}\frac{\partial u}{\partial z} + \frac{w}{a^2} + \beta a^2 \frac{\partial^4 w}{\partial z^4} - \frac{\omega^2}{a^2\omega_a^2}w = \frac{(1-\nu^2)}{Eh}\left(p_{\mathrm{in}}(z) - p_{\mathrm{out}}(z)\right), \tag{1b}$$

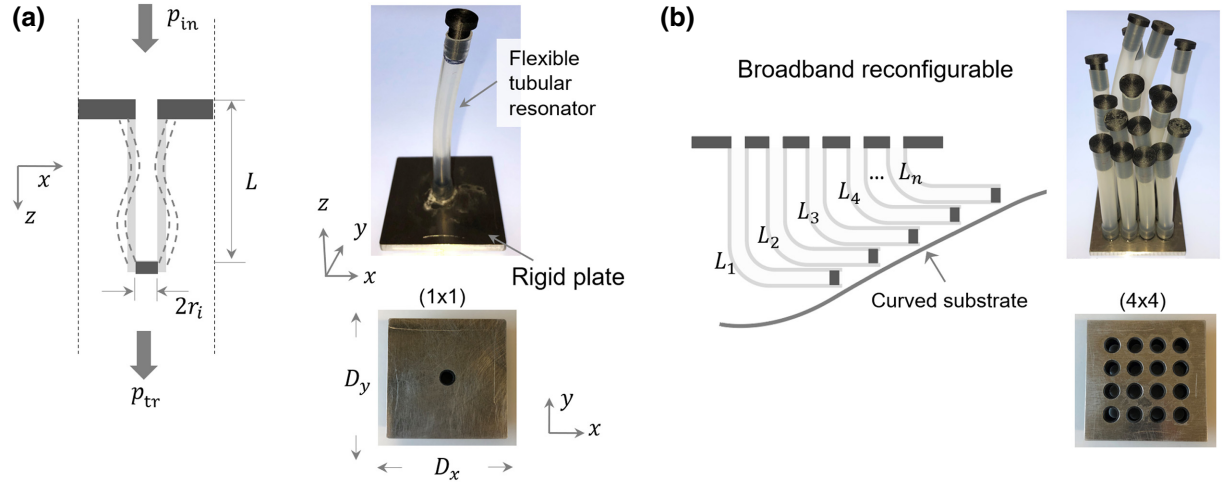

FIG. 1. Flexible tubular quarter-wavelength resonator. (a) Single-resonance absorber in the two-port system. The dimensions of the flexible tube are given by a length of L and an inner radius of r_i. (b) Multiple-resonance absorber system shaped for a structure of an arbitrary geometry. The photo shows the absorber composed of 16 tubular resonators (4×4) of variable lengths.

where $a = r_i + h/2$ is the effective radius (i.e., the middle of the shell), ω is the angular frequency, $p_{\text{in(out)}}$ is the pressure inside (outside) of the tube, $\beta = h^2/12a^2$ and $\omega_a = (1/a)\sqrt{E/\left(\rho_s(1-\nu^2)\right)}$ with the material properties of the flexible tube (Young's modulus E, mass density ρ_s, and Poisson's ratio ν). Here, the displacements u, w depend on the z direction. Note that only the radial component [Eq. (1b)] is influenced by the net pressure acting on the lateral surface of the tube $p_{\text{in}} - p_{\text{out}}$. The flexible tube is imposed by a simply supported boundary condition at both ends ($z = 0, L$), allowing us to obtain an analytical closed-form solution for physical insights into the system characteristics.

To characterize the structural modes induced by the acoustic waves, the shell displacement field ($\mathbf{X}$) is represented as a linear combination of modes Φ_q (q being a modal index) with the modal amplitudes A_q [30]: $\mathbf{X} = [u \;\; w]^T = \sum_{q=1}^{\infty} A_q \Phi_q$, with $\Phi_q = [U_q \cos(q\pi z/L) \;\; W_q \sin(q\pi z/L)]^T$. Here, Φ_q is expressed as axisymmetric modes (breathing modes) without considering fluid loading (also called *in vacuo* modes). By implementing the modal expansion and removing the external forces, the characteristic equation in a matrix form is constructed to calculate the natural frequency ω_q and corresponding modal mass m_q (see Appendix A). The shell motion equation expressed with the natural modal frequency ω_q is given by

$$\rho_s h \sum_q (-\omega^2 + \omega_q^2) A_q \Phi_q = P, \tag{2}$$

with $P = [0 \;\; p_{\text{in}} - p_{\text{out}}]^T$ acting on the lateral surface S. By using the orthogonal property of the modal basis functions, the motion equation for a specific mode q is expressed by

$$m_q(-\omega^2 + \omega_q^2) A_q = \langle P|\Phi_q\rangle, \tag{3}$$

where $\langle P|\Phi_q\rangle = \int_S P^T \Phi_q dS = 2\pi a \int_0^L \left[p_{\text{in}}(z) - p_{\text{out}}(z)\right] \sin(q\pi z/L) dz$. By using Green's function approach, $p_{\text{in(out)}}$ is expressed with the modal amplitude A_q and then is plugged into Eq. (3) for determining A_q and consequently $p_{\text{in(out)}}$ (see Appendix C).

For negligible transmission ($p_{\text{out}} \approx 0$) and the acoustic normal velocity V_0 at $z = 0$, the pressure inside the tube is given by $p_{\text{in}}(z) = p_{\text{QWR}}(z) + \sum_q p_q(z)$ with the acoustic modes (QWR) and structural modes (q). The acoustic impedance of the tube at $z = 0$ is calculated by $Z_{\text{tube}} = p_{\text{in}}(z=0)/V_0 = Z_{\text{QWR}} + \sum_q Z_q$. Therefore, the absorption (power) coefficient ($A = 1 - R$) of the flexible tube in a waveguide ($D_x = D_y = D$) is characterized by

$$A = 1 - \left|\frac{Z_0 - Z_s}{Z_0 + Z_s}\right|^2, \tag{4}$$

with $Z_s = (Z_{\text{QWR}} + \sum_q Z_q)(D^2/\pi r_{\text{in}}^2)$ and $Z_0 = c\rho_f$ with ρ_f being the air density. Here, derivation of Z_q and Z_{QWR} are found in Appendix B. For an absorber having multiple tubes (M being the number of the tubes), the overall surface impedance is derived as $Z_s = \left(\sum_{m=1}^{M} (\sigma_m/Z_{s,m})\right)^{-1}$ with $\sigma_m = \pi r_{\text{in},m}^2/D^2$ [31].

B. Hybrid resonances by interplay between acoustic and structural modes

Figure 2(a) illustrates the resonance modes supported by the flexible tube, showing the first QWR mode ($n = 1$) and a few structural resonance modes ($q = 1, 2, 3$). For a rigid tube, the QWR mode is dictated by vibrating air mass inside the tube and its compressibility ($\kappa = 1/\rho_f c^2$). For a tube having yielding walls in response to pressure, the compression of the air inside the tube is diluted, leading to a decrease in effective sound speed (c_e). Therefore, the frequency of QWR for the flexible tube is given by [32]

$$f_{\text{QWR}} = \frac{c_e}{4L_{\text{eq}}} = \frac{c}{4L_{\text{eq}}}\sqrt{\frac{K_w}{K_w + \rho_f c^2}} = f_{\text{QWR}}^o \sqrt{\frac{K_w}{K_w + \rho_f c^2}}, \tag{5}$$

where f_{QWR}^o ($=4/cL_{\text{eq}}$) is the QWR frequency of a rigid tube ($E > 1$ GPa), c_e is the effective sound given by $c_e = c\sqrt{K_w/(K_w + \rho_f c^2)}$ (see Supplemental Material [33]), $L_{\text{eq}} = L + \Delta L$ with the end correction ($\Delta L = \alpha r_i$), and K_w is the wall stiffness defined as the ratio between the pressure p and the fractional change in the cross-section area of the tube induced by p, i.e., $K_w = p/(\Delta S/S)$. Here, K_w is given by $K_w = Eh/2r_i$ with E being the elastic modulus of the tube and h being the tube wall thickness. Dependence of the QWR frequencies on E is shown in Fig. 2(b) (see the black solid line) for a tube ($L = 80$ mm, $h = 1$ mm, and $r_i = 3.5$ mm). Note that the QWR frequencies decrease with E because of a reduced effective sound speed. For a tube with a yielding wall ($E = 1$ MPa), $K_w = (Eh/2r_i) \approx \rho_f c^2$, and $f_{\text{QWR}} \approx 0.7 f_{\text{QWR}}^o$. For a rigid wall ($K_w \gg \rho_f c^2$), $K_w/(K_w + \rho_f c^2) \approx 1$, and $f_{\text{QWR}} \approx f_{\text{QWR}}^o$. Also plotted are the frequencies corresponding to the structural modes $q = 1, 2$, and 3 (dashed lines), which are analytically calculated from the eigenanalysis (see Appendix A). For specific elastic moduli (highlighted by the circle symbols), the QWR acoustic modes f_{QWR} coincide with the structural modes f_q. In this case, the absorption spectra, analytically calculated from Eq. (4), exhibit an interesting feature associated with the interaction between the acoustic and structural modes, as shown in Fig. 2(c) for complex elastic modulus $E = E_0(1 - \eta i)$ with the structural loss $\eta = 0$ (top) and 0.2 (bottom). Note that for no structural damping $\eta = 0$ (top), the absorption peaks split for $f_{\text{QWR}} = f_q$. In contrast, for considerable structural damping $\eta = 0.2$, the peak absorption line corresponding to f_{QWR} is observed to be

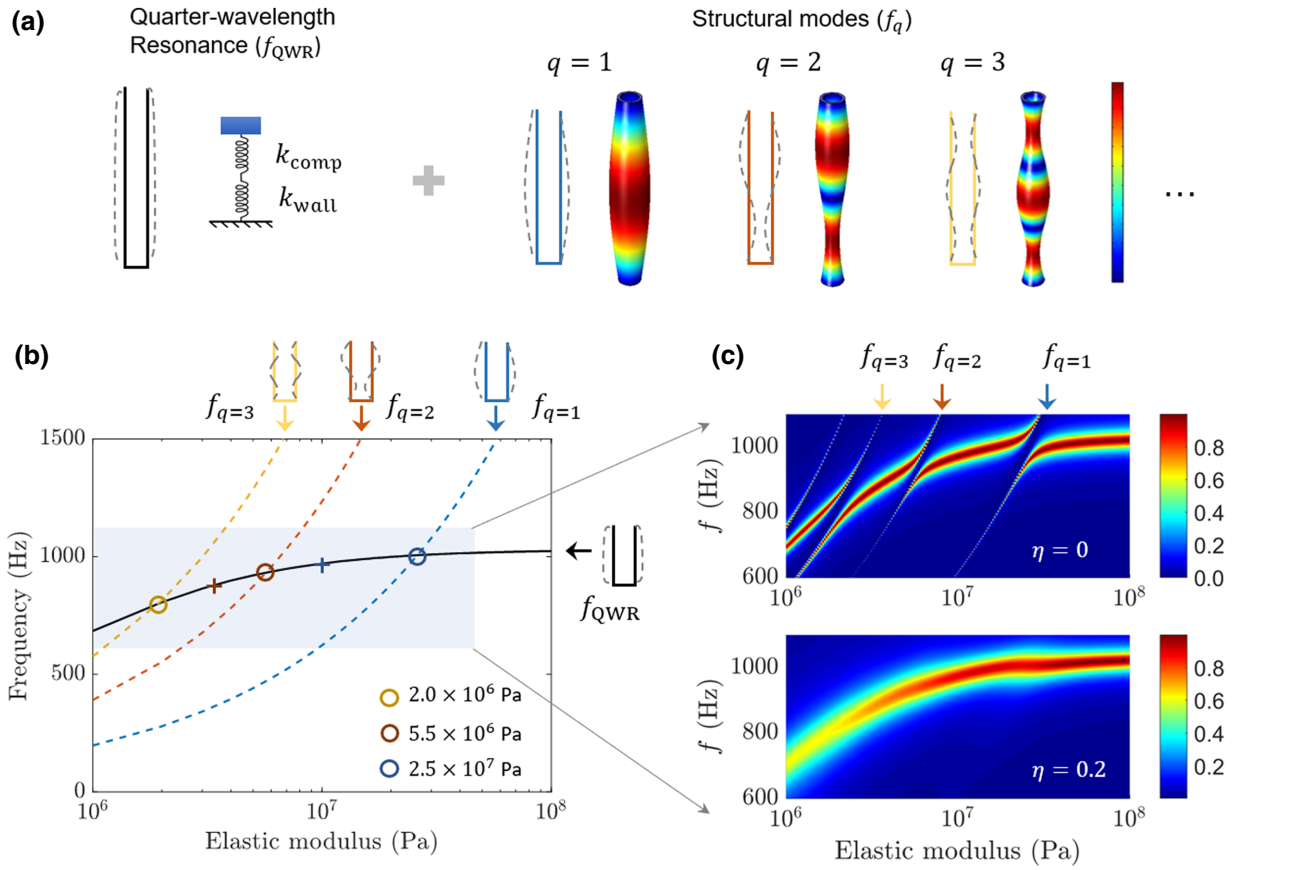

FIG. 2. Effect of the structural rigidity on acoustic absorption. (a) Resonance modes supported by flexible tubular resonators: quarter-wavelength acoustic resonance ($f_{QWR} \approx 0.25 c_e/L_{eq}$) and structural resonances (f_q with q being the mode index). (b) Analytically calculated resonance frequencies of the tubes ($L = 80$ mm, $r_i = 3.5$ mm) as a function of E_0. The specific elastic moduli for $f_{QWR} = f_q$ are indicated by the circle symbols. (c) Analytically calculated absorption with respect to E_0 for no structural damping $\eta = 0$ (top) and $\eta = 0.2$ (bottom).

continuous, indicating that the structural modes are highly suppressed by the structural loss.

To further understand the interplay of the acoustic mode and structural modes for $f_{QWR} \approx f_q$, the absorption spectra in the case of no structural damping are plotted in Fig. 3 for representative elastic moduli $E_0 = 4.5$, 5.5, 7.1, and 25 MPa. The analytical results (solid lines) using Eq. (4) show the excellent agreement with the numerical results (dashed lines) obtained from a numerical simulator (COMSOL Multiphysics 5.3a), proving the validity of the analytical model based on negligible transmission. In COMSOL simulation, the acoustic-structure interaction is solved by implementing a fully coupled model consisting of acoustics and solid mechanics modules in three-dimensional space without imposing an axisymmetric vibration condition. The rigid plate and adaptors are modeled as rigid domains while a simply supported boundary condition is applied to the tube ends (see Supplemental Material [33] for other boundary conditions). In Figs. 3(a) and 3(b), frequencies f_{QWR} for $E_0 = 5.5$ and 25 MPa coincide with $f_{q=2}$ and $f_{q=1}$, respectively, which are located between the two absorption peaks. Instead of a single peak having resonance degeneracy, the two peaks of the similar bandwidth appear due to the strong resonance mode coupling characterized as so-called Rabi splitting [34], where resonators exchange their energy much faster than it leaks or is dissipated, i.e., coupling rate, $g >$ loss rate, γ (see Supplemental Material [33] for further discussion). For $E_0 = 4.5$ and 7.1 MPa, the sharp absorption peaks (narrow band) corresponding to the structural modes f_q are placed slightly away from f_{QWR}, as observed in Figs. 3(c) and 3(d). In this weak-coupling regime, where the effective coupling between the resonance modes decreases due to detuning despite unchanged coupling strength (g), the structurally induced absorption spectra are similar to an asymmetric line shape observed in a Fano resonance describing interference between two scattered waves, e.g., wide-band wave (background) scattering and narrow-band resonant scattering [34]. In this case, the QWR mode as the background scattering decreases its amplitude slowly for frequencies away from f_{QWR}, interacting with the structural mode having a rapid phase variation. Furthermore, the

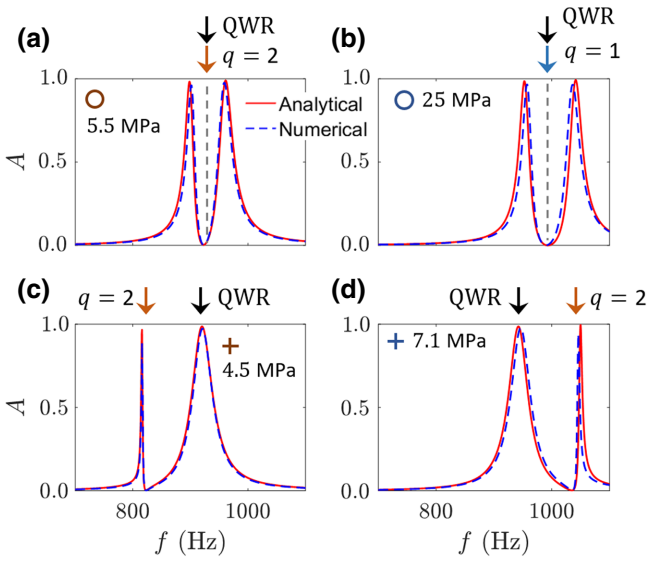

FIG. 3. Hybrid resonances for acoustic absorption. Absorption spectra of the tubes ($L = 80$ mm, $r_i = 3.5$ mm, and $\eta = 0$) with different elastic moduli. (a) Rabi splitting for $E_0 = 5.5$ MPa and $f_{q=2} = f_{\mathrm{QWR}}$, (b) Rabi splitting for $E_0 = 25$ MPa and $f_{q=1} = f_{\mathrm{QWR}}$. (c) Fano resonance for $E_0 = 4.5$ MPa and $f_{q=2} < f_{\mathrm{QWR}}$ (d) Fano resonance for $E_0 = 7.1$ MPa and $f_{q=2} > f_{\mathrm{QWR}}$. The solid lines indicate the analytical results while the dashed lines indicate the numerical results (COMSOL).

position of the structural mode ($q = 2$) with respect to the acoustic QWR modes varies depending on E, exhibiting $f_{\mathrm{QWR}} > f_{q=2}$ for 4.5 MPa and $f_{\mathrm{QWR}} < f_{q=2}$ for 7.1 MPa. For no structural damping ($\eta = 0$), the perfect absorption observed for the structural modes results from thermoviscous loss inside the tube, which also serves as a mechanism for QWR-induced absorption.

We investigate the effect of the structural damping η on hybrid resonances and acoustic absorption. Figure 4 shows the simulated absorption spectra of the flexible tube ($r_i = 3.5$ mm and $L = 80$ mm) for different structural dampings ($\eta = 0$, 0.025, and 0.05). For a relatively low rigidity of $E_0 = 2.65$ MPa, the absorption spectra exhibit sharp absorption peaks corresponding to a structural mode of $q = 3$ as well as those of QWR, as shown in Fig. 4(a). Both peaks for f_{QWR} and f_q decrease with η. Notably, the structural modes are more sensitive to the change in the structural damping. Interestingly, the QWR absorption is not always decreased by increasing η. Instead, the structural damping can enhance acoustic QWR absorption for larger r_i, as the peak absorption of QWR is plotted as a function of r_i in Fig. 4(b). For no structural damping $\eta = 0$ and $D = 50$ mm, the peak absorption of QWR is maximized with $r_i = 3.5$ mm, meeting the critical coupling, which states that the energy loss is balanced with the energy leakage [35]. For $r_i < 3.5$ mm, the loss is greater than the leakage (overdamped), whereas for $r_i > 3.5$ mm, the loss is smaller than the leakage (overleakage). Particularly, the overleakage cases for $r_i > 3.5$ mm benefit from the structural damping $\eta > 0$ by effectively increasing the overall loss for the critical coupling, as the optimized structural damping (top panel) and the corresponding peak absorption (blue star symbols in the bottom panel) are plotted in Fig. 4(b). For a certain case where the structural mode results in low absorption due to the overcoupling condition, increasing the structural damping leads to an enhanced acoustic absorption (see Supplemental Material [33]).

Unlike the analytical model with an assumption of negligible transmission, the numerical simulation (COMSOL) characterizes wave transmission, as shown in Fig. 4(c) for no structural damping $\eta = 0$. Particularly, when $E_0 < 5.5$ MPa (very soft), it is observed that the acoustic modes cause considerable acoustic transmission. Regardless of the elastic modulus, all the structural modes result in acoustic transmission. It is noted that for structural modes of odd number q, structurally induced transmission is observed when $f_{\mathrm{QWR}} > f_q$, whereas such transmission is also seen for the structural mode of even number q and $f_{\mathrm{QWR}} < f_q$. In Fig. 4(d), we observe that the presence of the structural damping ($\eta = 0.1$) eliminates acoustic transmission. In addition, the thickness and radius of the tube absorber have a critical effect on acoustic transmission (see Supplemental Material [33]).

C. Broadband absorber with multiple flexible quarter-wavelength resonators

The tube absorbers are experimentally characterized by using the four-microphone measurement [36] (see Supplemental Material [33]), as illustrated in Fig. 5(a). One end of the impedance tube ($D_x = D_y = 50$ mm) is connected by a loudspeaker generating acoustic waves in a frequency range of 600–1600 Hz, and the other end is closed by a 3D-printed cap with an anechoic termination. The tube resonators are fabricated with commercially available clear plastic PVC tubes (manufactured by Kesoto): three types of different E_0 (soft, moderate, hard). The other plastic parts including the adapters and end caps for the tube resonators are fabricated with a 3D printer (manufactured by Stratasys). For the single resonator experiment, all three types of the tube resonators have the same geometry: radius $r_i = 3.5$ mm, thickness $h = 1$ mm, and length $L = 90$ mm. The structural loss factors (η) and elastic moduli (E_0) of the tubes are extracted to be $\eta = 0.1$ and $E_0 = 17$, 54, and 72 MPa from numerical simulation. Figure 5(b) shows the acoustic spectra of the single-tube absorber having a relatively low rigidity ($E_0 = 17$ MPa), i.e., soft resonator. Note that the peak absorption corresponding to the QWR mode is observed to be 75% and its frequency is 850 Hz, compared to 920 Hz for a very high rigidity (dashed line). As increasing the rigidity to $E_0 = 54$ and

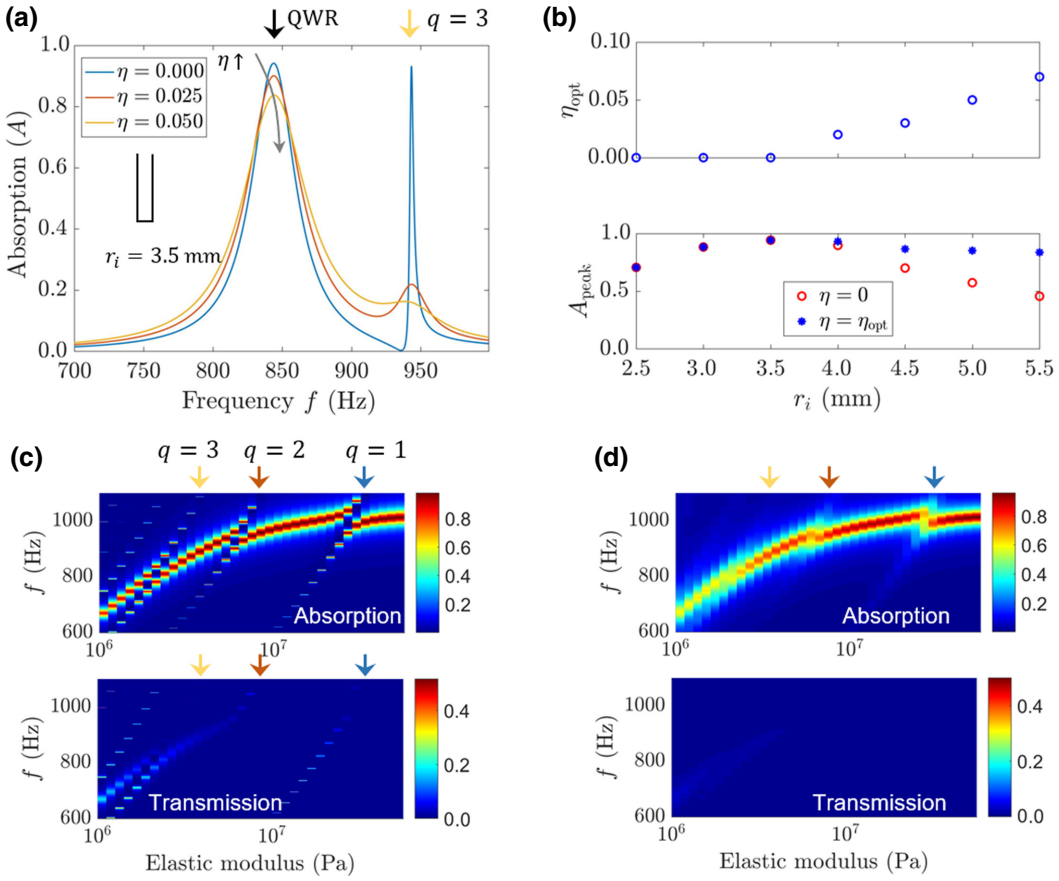

FIG. 4. Effect of the structural damping on acoustic absorption. (a) Numerically-calculated absorption spectra of the tubes ($L = 80$ mm, $r_i = 3.5$ mm and $E_0 = 2.65$ MPa) for different structural dampings $\eta = 0$, 0.025, and 0.05. (b) Numerically-calculated peak absorption of the tubes ($L = 80$ mm and $E_0 = 2.65$ MPa) as a function of r_i for no structural damping $\eta = 0$ and the optimized structural damping $\eta = \eta_{\rm opt}$. (c),(d) Numerically-calculated absorption (top) and transmission (bottom) with respect to elastic modulus E_0 for no structural loss $\eta = 0$ (c) and a structural loss of $\eta = 0.1$ (d).

72 MPa, the resonance frequency approaches 920 Hz, as shown in Figs. 5(c) and 5(d). The smaller peak absorption (850 Hz) observed in the soft tube [Fig. 5(b)] is attributed to an increased total damping ($c_{\rm loss} = c_{\rm loss,aco} + c_{\rm loss,str}$) due to the structural loss ($c_{\rm loss,str}$ and $\eta = 0.1$) for constant acoustic damping ($c_{\rm loss,aco}$). For $E_0 = 17$ MPa, the structural mode ($q = 1$) is estimated to be located at 650 Hz, showing its peak absorption of 10% in the measurement (highlighted by the vertical arrow). For relatively rigid tubes $E_0 = 54$ and 72 MPa, the structural modes are not observed in the frequency range, as they are located in high frequencies (>1500 Hz). For a straight tube geometry, the thickness of the absorber device is approximately 0.22λ, while a tube resonator having a coiled geometry permits a much smaller device thickness. Such a curved geometry changes acoustic performance [37], and the cross-section shape of the resonator influences the device performance (see Supplemental Material [33]).

The acoustic absorption induced by the structural mode is observed to be very low [Fig. 5(b)], because the energy loss rate $c_{\rm loss}$ is much greater than the energy leakage rate $c_{\rm leak}$ ($c_{\rm loss} \gg c_{\rm leak}$). To clearly see the structural mode ($q = 1$) in the absorption spectrum, the leakage damping rate ($c_{\rm leak}$) needs to be increased, which is realized by either smaller impedance tube (D) or larger resonator (r_i) [16]. Alternatively, such an increase in $c_{\rm leak}$ is also achieved by implementing multiple identical resonators (N), which is equivalent to a smaller impedance tube (D^2/N), i.e., $c^N_{\rm leak} = Nc_{\rm leak}$. Figure 6 shows the measured absorption spectra for different numbers of the identical tube resonators ($N = 1$, 4, and 8). The absorption peaks corresponding to the structural mode ($q = 1$) are enhanced to approximately 50% for $N = 8$, which is still low due to the overdamped condition. For the acoustic mode (QWR) and $N = 4$, the increased leakage rate leads to the critical coupling, showing the near-perfect absorption. Further increasing $c^N_{\rm leak}$ by $N = 8$ decreases the peak absorption at $f_{\rm QWR}$ to 90% due to the overcoupled condition ($c^{N=8}_{\rm leak} > c_{\rm loss}$). The dashed lines indicate the absorption spectra obtained from the harmonic oscillator (HOS) model with

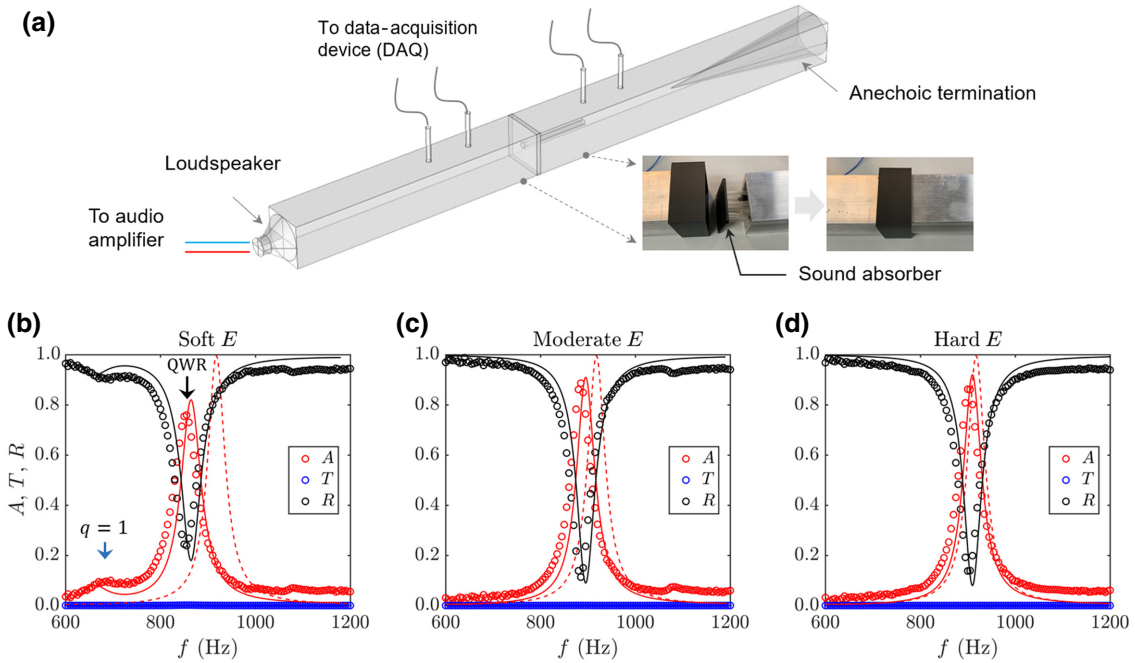

FIG. 5. Experimental results of the tube absorbers. (a) Illustration of the experimental setup consisting of four microphones. (b) Characterization of the single soft resonator ($E_0 = 17$ MPa). The experimental results (symbols) are compared with the COMSOL results (solid lines). The dashed lines indicate the simulation result for a tube of a high rigidity ($E_0 = 1$ GPa). The inset photo shows the device. (b) Spectra of the single resonator having a moderate rigidity ($E_0 = 54$ MPa). (c) Spectra of the single hard resonator ($E_0 = 72$ MPa).

the fitting parameters (see Appendix D). This HOS model enables us to check the balance between c_{loss} and c_{leak}. It is found that for $N = 1$, the acoustic mode (QWR) is $c_{\text{loss,QWR}} \approx 3c^{N=1}_{\text{leak,QWR}}$ with $c^{N=1}_{\text{leak,QWR}} = Z_0((\pi r_i^2)^2/D^2)$ whereas the structural modes are under the extremely overdamped condition, i.e., $c_{\text{loss},q=1} \approx 200c^{N=1}_{\text{leak},q=1}$ with $c^{N=1}_{\text{leak},q=1} = 0.3c^{N=1}_{\text{leak, QWR}}$. As shown in Fig. 6(b), the peak absorption for the acoustic and structural modes are plotted for N. The symbols indicate the measurement results whereas the solid lines indicate the results obtained from $c^N_{\text{leak}} = Nc_{\text{leak}}$ and the HOS model with the fitting values for $N = 1$.

To achieve broadband absorption, multiple tube resonators of different lengths are implemented [9,10]. Figure 7(a) exhibits the measured spectra of the 16 soft tubes ($E_0 = 17$ MPa) of the same diameter ($r_i = 3.5$ mm). High absorption ($> 70\%$) is observed for a wide range of frequencies 600–1250 Hz, which is shifted by 100 Hz with respect to the rigid tubes (dashed line). With the rigid tubes ($E_0 = 72$ MPa), the measured spectra are plotted in Fig. 7(b) for frequencies from 700 to 1400 Hz. The measured spectra of the rigid tubes show good agreement with the simulated spectra. Here, for the experiment, the lengths of the tubes for the soft and hard systems are given with 57.1, 60.1, 62.5, 65.2, 68.0, 72.3, 75.0, 78.9, 82.3, 86.4, 90.1, 94.2, 97.8, 103.5, 108.2, and 112.0 mm.

D. Duct silencer with flexible quarter-wavelength resonators

The flexible tube resonators are further implemented for a duct silencer, as illustrated in Fig. 8(a). Owing to its flexibility, the tube resonator can readily wrap around the duct for a compact design. In such a duct [one-dimensional (1D) waveguide], the single resonator with no loss is known to effectively suppress the transmission by reflecting all the incoming acoustic waves. However, in such a two-port system, the absorption of this single resonator is typically limited to 50% even with an optimized loss, thus requiring resonance degeneracy for the perfect absorption [15,38]. We consider dual resonances by using two flexible tube resonators attached to a circular duct (diameter $D = 70$ mm), as illustrated in Fig. 8(a). Here, the upstream resonator (L_1) is spaced with a distance of d from the downstream resonator (L_2). To build duct silencers, the hard tube ($E_0 = 72$ MPa) is chosen for minimum wave transmission across the resonator wall, and its sound loss for absorption is controlled dominantly by the acoustic loss ($c_{\text{loss,aco}}$) due to the negligible structural loss by the rigid tubes ($c_{\text{loss,aco}} \gg c_{\text{loss,str}}$).

In the numerical simulation, while the diameter of the resonators ($2r_i = 15$ mm) remains the same, we vary their distance (d) and lengths ($\Delta = L_2 - L_1$ for constant $L_1 =$ 100 mm). Figure 8(b) shows a surface plot of the highest

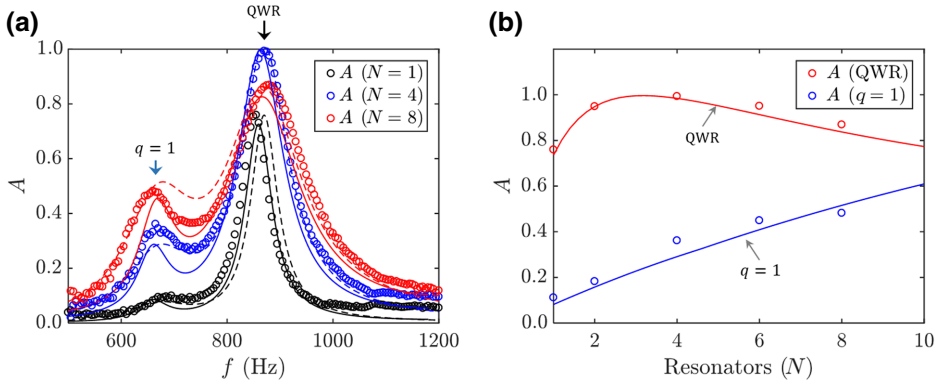

FIG. 6. Experimental characterization of structural resonance mode. (a) Absorption spectra for multiple identical resonators (N). The symbols indicate the experimental results and the solid lines denote the COMSOL results while the dashed lines indicate the results from the harmonic oscillator modes with fitting values. (b) Peak absorption for different numbers of the resonators.

absorption and lowest transmission in the calculated spectra for d and Δ. The maximum absorption is observed for $\Delta \approx 2$ mm and $d = 40$ mm [marked as the star symbol in Fig. 8(b)]. The longer downstream resonator leads to detuned resonance frequencies, and the corresponding detuning is characterized by $\Delta f = (c/4)\{(1/L_1) - [1/(L_1 + \Delta)]\} \approx 17$ Hz, compared to the bandwidth of 37 Hz. In addition, the distance $d = 40$ mm corresponds to 0.095λ. As shown in Fig. 8(c), the observed peak absorption corresponds to the zero reflection condition. The simulation results (symbols) show good agreement with the analytical results based on a harmonic oscillator model (HOM) (see Appendix D), which explicitly describes the coupling between the upstream and downstream resonators through $c_{\text{coup}} = \exp(-j\,\phi_p)c_{\text{leak}}$ with $c_{\text{leak}} = \frac{1}{2}Z_0[(\pi r_i^2)^2/\pi(D/2)^2]$. From the HOM, we find that the zero reflection condition is met by destructively cancelling the radiated waves from the upstream and downstream resonators (see Supplemental Material [33]). Here, the cancellation condition of the radiated waves is described by $|\arg(\dot{x}_1) - \arg(\dot{x}_2)| + \phi_p = n\pi$ with the upstream (downstream) resonator $x_{1(2)}$ and its phase angle $\arg(\dot{x}_{1(2)})$. We confirm that a sufficiently large phase difference of $|\arg(\dot{x}_1) - \arg(\dot{x}_2)|$ is enabled by both the coupling between the resonators ($\phi_p = 2\pi/\lambda d$) and resonance detuning ($\Delta f \propto \Delta$).

As indicated in Fig. 8(b), the condition for the maximum absorption (start symbol) is slightly different from the condition for the minimum transmission ($\Delta = 0$ mm and $d = 38$ mm), where no detuning is implemented. Under this minimum-transmission condition, the peak absorption is not that high (approximately 70%), whereas the transmission is significantly suppressed as low as $< 1\%$, as shown in Fig. 8(c). Also, note that when the identical resonators are used (i.e., $\Delta = 0$ mm), relatively low transmission is observed for a wide range of d. This is because each isolated resonator leads to small transmission (<10%). In Figs. 8(c) and 8(d), the numerical results (symbols) show good agreement with the analytical results from the harmonic oscillator model.

We experimentally characterized the acoustic performance of the fabricated duct silencer located in the middle of a circular duct, as shown in Fig. 9(a). The fabricated device is composed of six pairs of the flexible resonators ($2r_i = 15$ mm). Here, each resonator is connected into a hole via an angled adaptor and is ended by a rigid cap. We choose the condition for the minimum transmission [$\Delta = L_1 - L_2 = 0$ mm highlighted in Fig. 8(b)] such that the lengths in each pair are identical ($L_1 = L_2$). While we vary the lengths of the pairs for broadband transmission reduction, the distance for all the pairs remains the same ($d = 70$ mm). This is because the selection of the same

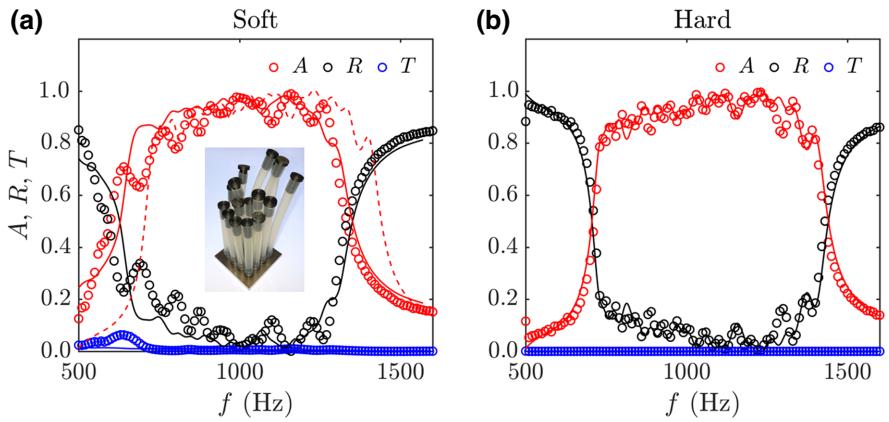

FIG. 7. Experimental characterization of broadband flexible tube absorbers. (a) 16 soft resonators ($E_0 = 17$ MPa). (b) 16 hard resonators ($E_0 = 72$ MPa). The symbols indicate the measurement results while the solid lines indicate the COMSOL results. The dashed line is the same as the solid line for the hard tubes.

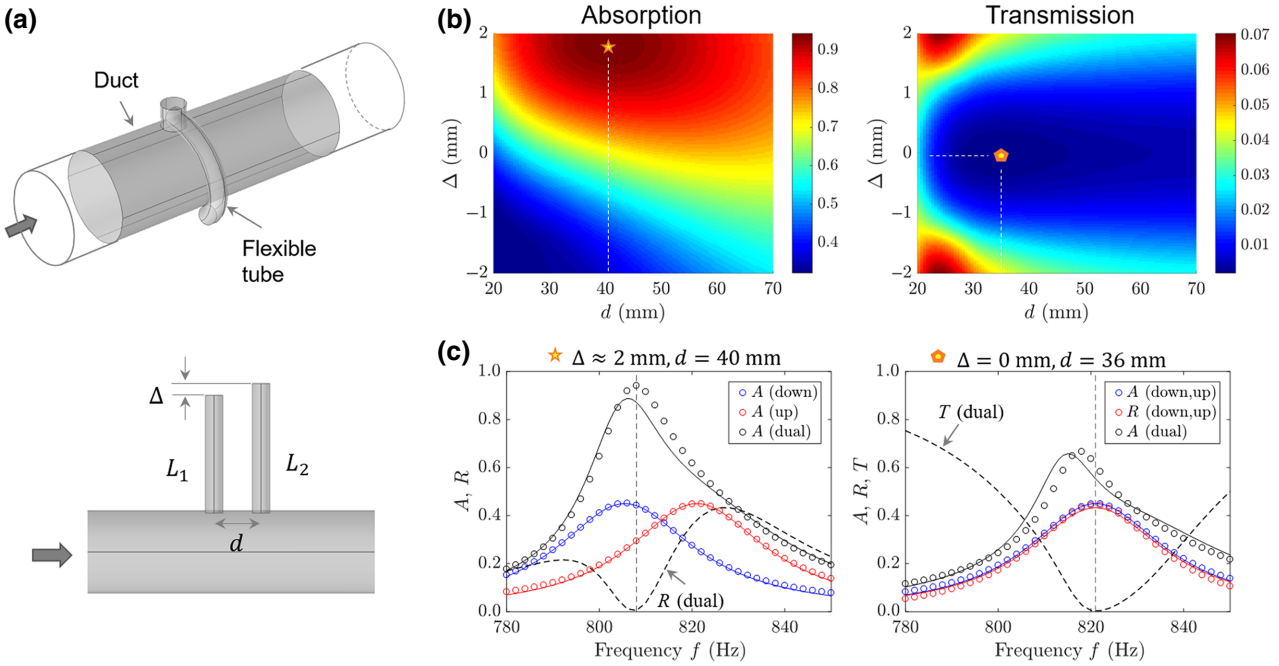

FIG. 8. Duct silencers made of flexible resonators. (a) Schematic of a duct (top) wrapped by a flexible tube and a duct (bottom) with two resonators of different lengths (upstream l_1 and downstream l_2). The distance between the resonators is given by d. (b) Simulation results of the duct silencer with one pair of resonators of the same diameter ($2r_i = 7$ mm) by varying l_1 and l_2 ($\Delta = l_2 - l_1$) and distance (d) at resonance frequencies. The highest absorption and lowest transmission are highlighted by the yellow star and pentagon, respectively. (c) Calculated spectra for the peak absorption ($\Delta \approx 2$ mm, $d = 40$ mm) and the minimum transmission ($\Delta = 0$ mm, $d = 36$ mm). The results for the coupled dual resonators are indicated by dual, while the isolated, uncoupled upstream and downstream resonators are indicated by up and down. The analytical results (solid lines) obtained from Eq. (D3) are compared with the simulation results (symbols). The dashed lines indicate the simulated reflection spectrum and transmission spectrum for the dual resonators.

distance does not critically influence the acoustic performance but it allows simple fabrication. Figure 9(b) shows the absorption (A), transmission (T), and reflection (R) of the fabricated device. The measurement results show approximately 80% absorption for a range of 800–950 Hz. The broadband transmission suppression is also observed.

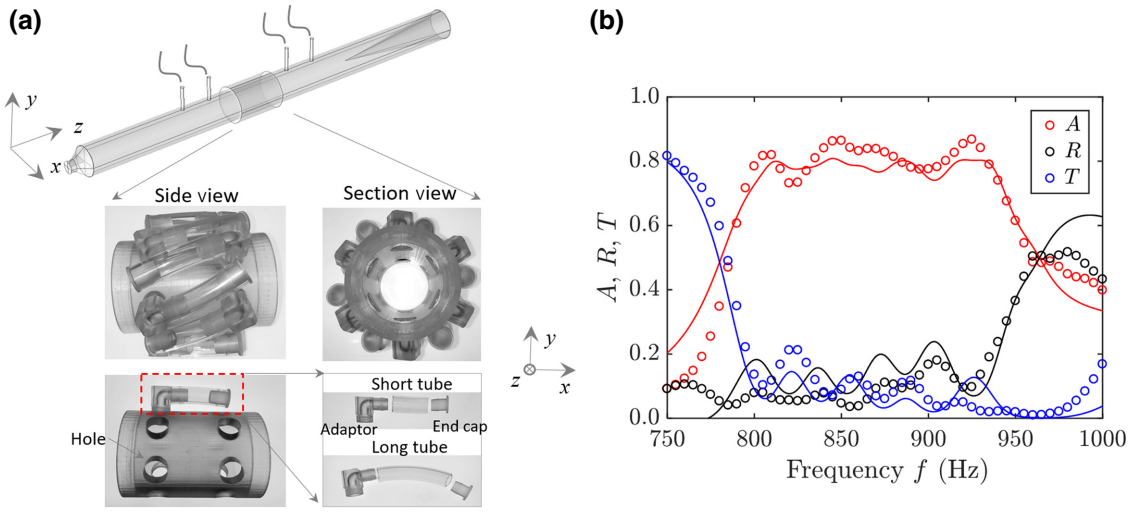

FIG. 9. Experimental characterization of duct silencers made of the flexible absorbers. (a) Photo of the fabricated duct silencer consisting of six pairs of the flexible resonators. (b) Acoustic absorption (A), transmission (T), reflection (R) spectra of the duct silencer. The numerical results (solid lines) are compared with the measurement results.

The simulation results (solid lines) show good agreement with the measurement results (symbols). Here, the lengths of the tubes are given by 85.0, 88.0, 91.0, 94.0, 97.0, and 110.0 mm. The performance can be further improved by adding more resonator pairs.

III. CONCLUSION

We show reconfigurable tube resonators made of soft, flexible materials for broadband sound absorption. We construct two types of acoustic absorbers consisting of flexible tube resonators. One is the wall-type acoustic absorber and the other is the duct-type absorber. Both types of absorbers exhibit broadband absorption by implementing multiple resonators of different resonance frequencies. While the tubes used for quarter-wavelength acoustic resonators are flexible enough for reconfiguration, they are sufficiently rigid for acoustic resonances. The structural rigidity and loss of the elastic tubes have been systematically studied. For the flexible tubes having a relatively low rigidity, the structural modes are observed at frequencies comparable to f_{QWR} of the acoustic mode, leading to the interaction between the acoustic and structural modes and thus exhibiting the Rabi splitting and Fano resonance. Also, the compliant walls of the flexible tubes cause the acoustic QWR mode frequency f_{QWR} to be redshifted for a compact, low-frequency absorber. This work allows a thorough understanding of flexible acoustic resonators and provides a viable solution to mitigate noises in space-limited applications.

APPENDIX A: CALCULATION OF MODAL MASS

By inserting $\Phi_q = [U_q \cos(q\pi z/L) \;\; W_q \sin(q\pi z/L)]^T$ into Eq. (1) and removing the external forces, the characteristic equation in a matrix form is represented as

$$\begin{bmatrix} -\left(\frac{q\pi a}{L}\right)^2 + \left(\frac{\omega_q}{\omega_a}\right)^2 & \nu\left(\frac{q\pi a}{L}\right) \\ \nu\left(\frac{q\pi a}{L}\right) & -1 - \beta\left(\frac{q\pi a}{L}\right)^4 + \left(\frac{\omega_q}{\omega_a}\right)^2 \end{bmatrix} \begin{bmatrix} U_q \\ W_q \end{bmatrix} = \Delta \begin{bmatrix} U_q \\ W_q \end{bmatrix} = 0. \tag{A1}$$

By setting the determinant to zero (i.e., $|\Delta| = 0$), the natural frequency ω_q is obtained:

$$\left(\frac{\omega_q}{\omega_a}\right)^4 - K_2\left(\frac{\omega_q}{\omega_a}\right)^2 + K_0 = 0, \tag{A2}$$

where $K_0 = (1-\nu^2)(q\pi a/L)^2 + \beta(q\pi a/L)^6$ and $K_2 = 1 + (q\pi a/L)^2 + \beta(q\pi a/L)^4$.

With the determined ω_q from the equation above, the displacement amplitude U_q is related to W_q:

$$\frac{U_q}{W_q} = \frac{\nu(q\pi a/L)}{(q\pi a/L)^2 - (\omega_q/\omega_a)^2}. \tag{A3}$$

By setting $W_q = 1$ for U_q in Eq. (A3), the modal mass (m_q) is obtained from

$$\int_S \Phi_q^T \Phi_{q'} \rho_s h dS = m_q \delta_{qq'}, \tag{A4}$$

with $m_q = \rho_s h \pi a L (U_q^2 + W_q^2)$.

APPENDIX B: ACOUSTIC PRESSURE FIELD INSIDE THE SHELL

1. Governing equations for axisymmetric vibration response

In the shell motion equation, only the radial component [i.e., Eq. (1b)] is influenced by the acoustic pressure inside and outside the tube, whose governing equation is expressed as the Helmholtz equation,

$$(\Delta^2 + k^2) p_{\mathrm{in(out)}} = 0. \tag{B1}$$

For the acoustic region inside the tube, the acoustic normal velocity is given by $V(z=0,r) = V_0$ for $r = \sqrt{x^2+y^2} < r_i$, and $V(z, r=r_i) = \dot{w}(z)$ on the shell surface. By simultaneously solving Eqs. (1) and (B1) subject to the boundary conditions, the shell displacement field and acoustic pressure field are determined, allowing characterization of the acoustic performance.

Considering the tube vibration, the acoustic pressure for the inside and outside of the tube can be expressed as the Kirchchoff-Helmholtz integral by [32]

$$p(z) = \int_S \left[G \frac{\partial p}{\partial n} - p \frac{\partial G}{\partial n} \right] dS, \tag{B2}$$

with the unitary normal vector (**n**) to the cylinder in the outward direction. Assuming $p_{\mathrm{in}} \gg p_{\mathrm{out}}$, our derivation below focuses on a case of $p_{\mathrm{out}} \approx 0$ (i.e., negligible transmission). Since the tube size is much smaller than the wavelength, the acoustic pressure inside the tube is a one-dimensional plane wave [$p_{\mathrm{in}}(x,y,z) = p_{\mathrm{in}}(z)$]. Thus, Green's function G is given by [32]

$$G(z, z_0) = \frac{j}{2k\pi a^2} e^{jk|z-z_0|}. \tag{B3}$$

After combining Eqs. (B2) and (B3) and then applying the boundary conditions, the acoustic pressure inside the tube is represented by

$$p_{\mathrm{in}}(z) = [A^+ + B^+(z)] e^{jkz} + [A^- + B^-(z)] e^{jk(L-z)}. \tag{B4}$$

Here, A^+ and A^- are determined boundary conditions at $z = 0, L$, respectively, while $B^{+(-)}$ is obtained from the

lateral shell velocity. Here, A^+, A^-, $B^+(z)$, and $B^-(z)$ are expressed by

$$A^+ = \frac{j}{2k\pi a^2}\int_{S_0}(-j\,\rho_f\,\omega)V dS + \frac{j}{2\pi a^2}\int_{S_0} p dS = \frac{\rho_f\,c}{2}V(0) + \frac{p(0)}{2}, \tag{B5a}$$

$$A^- = \frac{j}{2k\pi a^2}\int_{S_L}(j\,\rho_f\,\omega)V dS + \frac{j}{2\pi a^2}\int_{S_L} p dS = -\frac{\rho_f\,c}{2}V(L) + \frac{p(L)}{2}, \tag{B5b}$$

$$B^+(z) = -\frac{\rho_f\,c}{a}\int_0^z e^{-jkz_0}\dot{w}(z_0)dz_0, \tag{B5c}$$

$$B^-(z) = -\frac{\rho_f\,c}{a}e^{-jkL}\int_z^L e^{jkz_0}\dot{w}(z_0)dz_0. \tag{B5d}$$

For the simply supported boundary condition, the lateral velocity of the shell is given by

$$\dot{w}(z) = -j\,\omega\sum_{q=1}^{\infty}A_q\sin(q\pi z/L). \tag{B6}$$

By plugging Eq. (B6) into Eqs. (B5c) and (B5d), the following equations are obtained:

$$B^+(z) = \frac{j\,\rho_f\,c\omega}{a}\sum_q\frac{A_q}{[k^2-(q\pi/2)^2]}\times\left[-\frac{q\pi}{L}+\left(jk\sin\left(\frac{q\pi}{L}z\right)+\frac{q\pi}{L}\cos\left(\frac{q\pi}{L}z\right)\right)e^{-jkz}\right], \tag{B7a}$$

$$B^-(z) = \frac{j\,\rho_f\,c\omega}{a}\sum_q\frac{A_q}{[k^2-(q\pi/2)^2]}\times\left[(-1)^q\frac{q\pi}{L}+\left(jk\sin\left(\frac{q\pi}{L}z\right)-\frac{q\pi}{L}\cos\left(\frac{q\pi}{L}z\right)\right)e^{jk(z-L)}\right]. \tag{B7b}$$

With $B^+(0) = B^-(L) = 0$, the pressure at both ends ($z = 0, L$) is expressed by

$$p(z=0) = A^+ + [A^- + B^-(0)]e^{jkL} \tag{B8a}$$

$$p(z=L) = [A^+ + B^+(L)]e^{jkL} + A^-. \tag{B8b}$$

By using Eqs. (B8), (B5a), and (B5b) with $V(z=L)=0$, A^+ and A^- are given by

$$A^+ = \frac{1}{e^{jkL}-e^{-jkL}}[-B^+(L)e^{jkL} - B^-(0) - \rho_f\,cV(0)e^{-jkL}], \tag{B9a}$$

$$A^- = \frac{1}{e^{jkL}-e^{-jkL}}[-B^+(L) - B^-(0)e^{jkL} - \rho_f\,cV(0)]. \tag{B9b}$$

With setting $V_0 = 0$ for the acoustic pressure generated by the shell vibration alone, A^+ and A^- are given by

$$A^+ = \frac{j\,\rho_f\,c\omega}{a}\sum_q\frac{A_q}{[k^2-(q\pi/2)^2]}\frac{[-(-1)^q+\cos(kL)]}{j\,\sin(kL)}\times\left(\frac{q\pi}{L}\right), \tag{B10a}$$

$$A^- = \frac{j\,\rho_f\,c\omega}{a}\sum_q\frac{A_q}{[k^2-(q\pi/2)^2]}\frac{[1-(-1)^q\cos(kL)]}{j\,\sin(kL)}\times\left(\frac{q\pi}{L}\right). \tag{B10b}$$

Thus, plugging Eq. (B10) into Eq. (B8) leads to

$$p_{\text{shell}}(z) = -\frac{2\rho_f\,c\omega}{a}\sum_q\frac{A_q}{[k^2-(q\pi/L)^2]}\times\left[\frac{(-1)^q\cos(kL)-\cos\left(k(L-z)\right)}{\sin(kL)}\left(\frac{q\pi}{L}\right)+k\sin\left(\frac{q\pi}{L}z\right)\right]. \tag{B11}$$

For the acoustic pressure generated by the rigid tube, we have $A_q = 0$, $V_L = 0$, $V_0 \neq 0$, and $B^+(z) = B^-(z) = 0$.

$$A^+ = \frac{-\rho_f\,cV_0e^{-jkL}}{e^{jkL}-e^{-jkL}}, \tag{B12a}$$

$$A^- = \frac{-\rho_f\,cV_0}{e^{jkL}-e^{-jkL}}. \tag{B12b}$$

By inserting Eqs. (B12) to (B8), the acoustic pressure for the rigid tube is represented by

$$p_{\text{rigid}}(z) = A^+e^{jkz} + A^-e^{jk(L-z)} = j\,\rho_f\,cV_0\frac{\cos\left(k(L-z)\right)}{\sin kL}. \tag{B13}$$

Therefore, by combining Eqs. (B11) and (B13), the acoustic pressure is given by

$$p(z) = p_{\text{rigid}}(z) + p_{\text{shell}}(z), \tag{B14}$$

with $p_{\text{shell}}(z) = \sum_{q=1}^{\infty} p_q(z)$. Alternatively, for a limited number N_q of structural modes (e.g., $N_q < 5$) in a frequency range of interest, the acoustic pressure is approximately calculated by

$$p(z) \approx p_{\text{QWR}}(z) + \sum_{q=1}^{N_q} p_q(z). \tag{B15}$$

p_{QWR} is based on acoustic modes considering a stiffness change due to the yielding wall, which is expressed by $p_{\text{QWR}}(z) = \beta p_{\text{rigid}}(z)$ with $\beta = \sqrt{K_w/(K_w + \rho_f c^2)}$ and K_w being the wall stiffness defined as a ratio between the pressure p and the fractional change in the cross-section area of the duct induced by p.

2. Acoustic impedance

From the acoustic pressure field $p_{\text{in}}(z)$, the acoustic impedance of the flexible tube at $z = 0$ is defined by

$$Z = Z_{\text{rigid}} + Z_{\text{shell}} = \frac{p_{\text{rigid}}(0)}{V_0} + \frac{p_{\text{shell}}(0)}{V_0}, \tag{B16}$$

with V_0 being the acoustic normal velocity at $z = 0$. The acoustic impedance Z_{rigid} is related to the equivalent channel length $L + \Delta L$, where ΔL is the end corrections to the length. The relation is shown by

$$Z_{\text{rigid}} = j\,\rho_f\, c\cot[k(L + \Delta L)]. \tag{B17}$$

Considering the wall compliance, the acoustic impedance for QWR is expressed by

$$Z_{\text{QWR}} = j\,\rho_f\, c\sqrt{\frac{K_w}{K_w + \rho_f c^2}}\cot[k(L + \Delta L)]. \tag{B18}$$

The acoustic impedance Z_{shell} corresponding to the structural modes is represented by

$$Z_{\text{shell}} = \frac{p_{\text{shell}(z=0)}}{V_0} = -\frac{2\rho_f\, c\omega}{aV_0}\sum_q A_q\left[(-1)^q - 1\right] \times \cot(kL)\frac{(q\pi/L)}{[k^2 - (q\pi/L)^2]}. \tag{B19}$$

The acoustic impedance Z_{shell} for the odd mode index $q = 2n - 1$ is simplified to

$$Z_{\text{shell}} = \frac{4\rho_f\, c\omega}{aV_0}\sum_{q=2n-1} A_q\cot(kL)\frac{(q\pi/L)}{[k^2 - (q\pi/L)^2]}. \tag{B20}$$

3. Thermoviscous acoustic loss

For acoustic dissipation inside small tubes, the narrow region acoustics model (circular duct) is implemented, which is characterized with complex sound speed (c_c) and complex density (ρ_c), respectively, [39]:

$$c_c = c\sqrt{\frac{\Psi_v}{\gamma - (\gamma - 1)\Psi_h}}, \tag{B21a}$$

$$\rho_c = \frac{\rho_f}{\Psi_v}, \tag{B21b}$$

with the specific heat ratio γ, $\Psi_n = -(J_2(r_i k_n)/J_0(r_i k_n))$ (for $n = v,\ h$), and J_m being the Bessel function of the first kind and order m. Here, $k_{v(h)}$ are given, respectively, by $k_v^2 = -j\,\omega(\rho_f/\mu)$ and $k_h^2 = -j\,\omega(\rho C_p/k_{\text{th}})$, which are determined with air properties: C_p heat capacity at constant pressure, k_{th} thermal conductivity, and μ dynamic viscosity. The narrow region acoustics model is validated for the cross section of the tube ($2r_i$) smaller than the acoustic wavelength (λ), constant cross section in the propagation direction, and the length of the tube (L) larger than the thermal (viscous) boundary layer thickness.

APPENDIX C: CALCULATION OF THE MODE AMPLITUDE A_q

Assuming $p_{\text{out}} = 0$, the motion equation is expressed by

$$m_q(-\omega^2 + \omega_q^2)A_q = 2\pi a\int_0^L p_{\text{in}}(z)\sin(q\pi z/L)dz \tag{C1a}$$

$$= 2\pi a\int_0^L [p_{\text{rigid}}(z) + p_{\text{shell}}(z)]\sin(q\pi z/L)dz. \tag{C1b}$$

For the finite number of vibration modes, the equation can be represented as a matrix form:

$$\begin{bmatrix} A_1 \\ A_2 \\ \vdots \\ A_N \end{bmatrix} = \begin{bmatrix} B_{11} & B_{12} & \cdots & B_{1N} \\ B_{21} & B_{22} & & B_{2N} \\ \vdots & & \ddots & \vdots \\ B_{N1} & B_{N2} & \cdots & B_{NN} \end{bmatrix}^{-1} \begin{bmatrix} C_1 \\ C_2 \\ \vdots \\ C_N \end{bmatrix}. \tag{C2}$$

Here, the elements of the matrices are expressed by

$$B_{qq'} = m_q(-\omega^2 + \omega_q^2)\delta_{qq'} - 2\pi a\int_0^L D_{q'}(z)\sin(q\pi z/L)dz, \tag{C3a}$$

$$C_q = 2\pi a\int_0^L p_{\text{rigid}}(z)\sin(q\pi z/L)dz, \tag{C3b}$$

with

$$D_q(z) = p_{\text{shell},q}/A_q = -\frac{2\rho_f c\omega}{a[k^2-(q\pi/L)^2]}\left[\frac{(-1)^q\cos(kL)-\cos\left(k(L-z)\right)}{\sin(kL)}\left(\frac{q\pi}{L}\right)+k\sin\left(\frac{q\pi}{L}z\right)\right]. \tag{C4}$$

With Eq. (B14) and vibration mode amplitudes calculated from Eq. (C2), the acoustic pressure field inside the shell is determined.

Without coupling between the modes, the single vibration mode amplitude is expressed by

$$A_q = \frac{2\pi a\int_0^L p_{\text{rigid}}(z)\sin(q\pi z/L)dz}{m_q(-\omega^2+\omega_q^2)-2\pi a\int_0^L D_q(z)\sin(q\pi z/L)dz}. \tag{C5}$$

APPENDIX D: HARMONIC OSCILLATOR MODEL FOR RIGID TUBES

1. One-port system

To alternatively investigate the acoustic performance of the rigid tubes supporting quarter-wavelength resonant modes, we also consider an analytical model based on a harmonic oscillator consisting of mass (m), damper (c), and spring (k). This formalism permits characterization of a system in terms of the critical coupling by explicitly representing the magnitude of each loss component. The motion of equation (x) is given by

$$m\ddot{x}+c\dot{x}+k = F\exp(i\omega t), \tag{D1}$$

where the force is exerted by the sound wave [$p_0\exp(i\omega t)$] on the mass of an area S_r (i.e., $F = 2p_0S_r$ for one port and $F = p_0S_r$ for two ports). Also, the damping coefficient is given by $c = c_{\text{loss}} + c_{\text{leak}}$ with the intrinsic loss c_{loss} and the radiation leakage c_{leak}. With the dissipated power ($P_{\text{diss}} = \frac{1}{2}c_{\text{loss}}\mid\dot{x}\mid^2$) and incident power [$P_{\text{inc}} = \frac{1}{2}(p_0^2S_{\text{inc}}/Z_0)$ with $S_{\text{inc}} = D^2$ and the acoustic impedance Z], the absorption spectrum (A) is represented by [16]

$$A = \frac{P_{\text{diss}}}{P_{\text{inc}}} = 4\delta c_{\text{leak}}^2\left|\frac{\omega j}{-m\omega^2+(1+\delta)c_{\text{leak}}\omega j+m\omega_0^2}\right|^2, \tag{D2}$$

where ω is the angular frequency, δ is the ratio of $c_{\text{loss}}/c_{\text{leak}}$, and ω_0 is the angular resonance frequency ($f_{\text{res}} = \omega_0/2\pi$). For $\omega = \omega_0$, the peak absorption is given by $A = 4\delta/(1+\delta)^2$. For $\delta = 1$, the critical coupling ($c_{\text{loss}} = c_{\text{leak}}$) is achieved, enabling perfect absorption ($A = 1$). By using Eq. (D2), the absorption spectrum is semianalytically calculated with fitting parameters of δ and m. With the experimentally obtained A_p, we determine δ through $A_p = 4\delta/(1+\delta)^2$ and thus $c_{\text{loss}} = \delta c_{\text{leak}}$ is calculated for the known $c_{\text{leak}} = Z_0[(\pi r_i^2)^2/D^2]$. Now, with A_p and δ, we determine $c = c_{\text{loss}} + c_{\text{leak}}$. From the resonance frequency f_0 of the absorption spectrum, k is calculated with a fitted value of m through $f_0 = 1/2\pi\sqrt{k/m}$. Or m is calculated with a fitted value of k.

2. Two-port system

For two-port systems (e.g., ducts), a resonance degeneracy based on two resonators is introduced to realize perfect acoustic absorption. Such a two-resonator system permits control of the resonance coupling by the distance (d) as well as resonance detuning by using the tubes of different lengths (L_1, L_2). The coupled equation of motion is expressed by [15,17]

$$\begin{bmatrix} m_1 & 0 \\ 0 & m_2 \end{bmatrix}\begin{bmatrix}\ddot{x}_1\\ \ddot{x}_2\end{bmatrix}+\begin{bmatrix}(1+\delta_1)c_{\text{leak}} & c_{\text{coup}}\\ c_{\text{coup}} & (1+\delta_2)c_{\text{leak}}\end{bmatrix}\begin{bmatrix}\dot{x}_1\\ \dot{x}_2\end{bmatrix} + \begin{bmatrix}k_1 & 0\\ 0 & k_2\end{bmatrix}\begin{bmatrix}x_1\\ x_2\end{bmatrix} = \begin{bmatrix}F\exp(i\omega t)\\ F\exp(i\omega t+i\phi_p)\end{bmatrix}, \tag{D3}$$

where the subscript 1(2) indicates the upstream (downstream) resonator, c_{coup} is the coupling constant, and ϕ_p is the propagation phase corresponding to d (i.e., $\phi_p = 2\pi\, d/\lambda$). Here, the coupling term for a circular waveguide (D diameter) is given by $c_{\text{coup}} = \exp(-i\phi_p)c_{\text{leak}}$ with $c_{\text{leak}} = 0.5Z_0[(\pi r_i^2)^2/\pi(D/2)^2]$. The absorption coefficient is expressed by

$$A = \frac{P_{\text{diss}}}{P_{\text{inc}}} = \left[\frac{1}{2}c_{\text{loss},1}|\dot{x}_2|^2+\frac{1}{2}c_{\text{loss},2}|\dot{x}_2|^2\right]/P_{\text{inc}}. \tag{D4}$$

[1] A. Climente, D. Torrent, and J. Sánchez-Dehesa, Omnidirectional broadband acoustic absorber based on metamaterials, Appl. Phys. Lett. **100**, 144103 (2012).

[2] J. Mei, G. Ma, M. Yang, Z. Yang, W. Wen, and P. Sheng, Dark acoustic metamaterials as super absorbers for low-frequency sound, Nat. Commun. **3**, 1 (2012).

[3] G. Ma, M. Yang, S. Xiao, Z. Yang, and P. Sheng, Acoustic metasurface with hybrid resonances, Nat. Mater. **13**, 873 (2014).

[4] X. Cai, Q. Guo, G. Hu, and J. Yang, Ultrathin low-frequency sound absorbing panels based on coplanar spiral tubes or coplanar Helmholtz resonators, Appl. Phys. Lett. **105**, 121901 (2014).

[5] Y. Liand and B. M. Assouar, Acoustic metasurface-based perfect absorber with deep subwavelength thickness, Appl. Phys. Lett. **108**, 063502 (2016).

[6] X. Peng, J. Ji, and Y. Jing, Composite honeycomb metasurface panel for broadband sound absorption, J. Acoust. Soc. Am. **144**, EL255 (2018).

[7] K. Donda, Y. Zhu, S.-W. Fan, L. Cao, Y. Li, and B. Assouar, Extreme low-frequency ultrathin acoustic absorbing metasurface, Appl. Phys. Lett. **115**, 173506 (2019).
[8] Z. Yang, H. Dai, N. Chan, G. Ma, and P. Sheng, Acoustic metamaterial panels for sound attenuation in the 50–1000 Hz regime, Appl. Phys. Lett. **96**, 041906 (2010).
[9] M. Yang, S. Chen, C. Fu, and P. Sheng, Optimal sound-absorbing structures, Mater. Horiz. **4**, 673 (2017).
[10] N. Jiménez, V. Romero-García, V. Pagneux, and J.-P. Groby, Rainbow-trapping absorbers: Broadband, perfect and asymmetric sound absorption by subwavelength panels for transmission problems, Sci. Rep. **7**, 1 (2017).
[11] H. Long, C. Liu, C. Shao, Y. Cheng, K. Chen, X. Qiu, and X. Liu, Subwavelength broadband sound absorber based on a composite metasurface, Sci. Rep. **10**, 1 (2020).
[12] C. Shao, Y. Zhu, H. Long, C. Liu, Y. Cheng, and X. Liu, Metasurface absorber for ultra-broadband sound via overdamped modes coupling, Appl. Phys. Lett. **120**, 083504 (2022).
[13] C. Chen, Z. Du, G. Hu, and J. Yang, A low-frequency sound absorbing material with subwavelength thickness, Appl. Phys. Lett. **110**, 221903 (2017).
[14] J. Ji, D. Li, Y. Li, and Y. Jing, Low-frequency broadband acoustic metasurface absorbing panels, Front. Mech. Eng. **6**, 94 (2020).
[15] T. Lee, T. Nomura, E. M. Dede, and H. Iizuka, Asymmetric loss-induced perfect sound absorption in duct silencers, Appl. Phys. Lett. **116**, 214101 (2020).
[16] T. Lee, T. Nomura, and H. Iizuka, Damped resonance for broadband acoustic absorption in one-port and two-port systems, Sci. Rep. **9**, 1 (2019).
[17] T. Lee, T. Nomura, E. M. Dede, and H. Iizuka, Ultrasparse Acoustic Absorbers Enabling Fluid Flow and Visible-Light Controls, Phys. Rev. Appl. **11**, 024022 (2019).
[18] X. Wu, K. Y. Au-Yeung, X. Li, R. C. Roberts, J. Tian, C. Hu, Y. Huang, S. Wang, Z. Yang, and W. Wen, High-efficiency ventilated metamaterial absorber at low frequency, Appl. Phys. Lett. **112**, 103505 (2018).
[19] X. Suand and D. Banerjee, Extraordinary Sound Isolation using an Ultrasparse Array of Degenerate Anisotropic Scatterers, Phys. Rev. Appl. **13**, 064047 (2020).
[20] M. Yang, C. Meng, C. Fu, Y. Li, Z. Yang, and P. Sheng, Subwavelength total acoustic absorption with degenerate resonators, Appl. Phys. Lett. **107**, 104104 (2015).
[21] S. Kumar, T. B. Xiang, and H. P. Lee, Ventilated acoustic metamaterial window panels for simultaneous noise shielding and air circulation, Appl. Acoust. **159**, 107088 (2020).
[22] X. Xiang, X. Wu, X. Li, P. Wu, H. He, Q. Mu, S. Wang, Y. Huang, and W. Wen, Ultra-open ventilated metamaterial absorbers for sound-silencing applications in environment with free air flows, Extreme Mech. Lett. **39**, 100786 (2020).
[23] H. Nguyen, Q. Wu, X. Xu, H. Chen, S. Tracy, and G. Huang, Broadband acoustic silencer with ventilation based on slit-type helmholtz resonators, Appl. Phys. Lett. **117**, 134103 (2020).
[24] S. Kumarand and H. P. Lee, Labyrinthine acoustic metastructures enabling broadband sound absorption and ventilation, Appl. Phys. Lett. **116**, 134103 (2020).
[25] Q. Wang, Y. Ge, H.-X. Sun, H. Xue, D. Jia, Y.-J. Guan, S.-Q. Yuan, B. Zhang, and Y. Chong, Vortex states in an acoustic Weyl crystal with a topological lattice defect, Nat. Commun. **12**, 1 (2021).
[26] S. Cuiand and R. L. Harne, Soft Materials with Broadband and Near-Total Absorption of Sound, Phys. Rev. Appl. **12**, 064059 (2019).
[27] M. H. Kurdi, G. Scott Duncan, and S. S. Nudehi, Optimal design of a Helmholtz resonator with a flexible end plate, J. Vib. Acoust. **136**, 031004 (2014).
[28] S. Cuiand and R. L. Harne, Acoustic-structure interaction in an adaptive Helmholtz resonator by compliance and constraint, J. Vib. Acoust. **142**, 021005 (2020).
[29] C. Fullerand and F. J. Fahy, Characteristics of wave propagation and energy distributions in cylindrical elastic shells filled with fluid, J. Sound Vib. **81**, 501 (1982).
[30] R. Pico, F. Gautier, and J. Redondo, Acoustic input impedance of a vibrating cylindrical tube, J. Sound Vib. **301**, 649 (2007).
[31] C. Shen, Y. Liu, and L. Huang, On acoustic absorption mechanisms of multiple coupled quarter-wavelength resonators: Mutual impedance effects, J. Sound Vib. **508**, 116202 (2021).
[32] P. M. Morseand, K. U. Ingard, *Theoretical Acoustics* (McGraw-Hill, New York, 1968).
[33] See Supplemental Material at http://link.aps.org/supplemental/10.1103/PhysRevApplied.18.014055 for schematics of experimental setups, and additional figures and notes.
[34] M. F. Limonov, M. V. Rybin, A. N. Poddubny, and Y. S. Kivshar, Fano resonances in photonics, Nat. Photonics **11**, 543 (2017).
[35] H. Long, Y. Cheng, J. Tao, and X. Liu, Perfect absorption of low-frequency sound waves by critically coupled subwavelength resonant system, Appl. Phys. Lett. **110**, 023502 (2017).
[36] M. Möser, *Engineering Acoustics* (Springer, London, 2009).
[37] T. Cambonie, F. Mbailassem, and E. Gourdon, Bending a quarter wavelength resonator: Curvature effects on sound absorption properties, Appl. Acoust. **131**, 87 (2018).
[38] H. Long, C. Liu, C. Shao, Y. Cheng, J. Tao, X. Qiu, and X. Liu, Tunable and broadband asymmetric sound absorptions with coupling of acoustic bright and dark modes, J. Sound Vib. **479**, 115371 (2020).
[39] H. Tijdeman, On the propagation of sound waves in cylindrical tubes, J. Sound Vib. **39**, 1 (1975).